Proceedings of ASME Turbo Expo 2016: Turbomachinery Technical Conference and Exposition
GT2016
June 13-17, 2016, Seoul, South Korea

GTP-16-1224

UNCERTAINTY QUANTIFICATION OF GROWTH RATES OF THERMOACOUSTIC INSTABILITY BY AN ADJOINT HELMHOLTZ SOLVER

Camilo F. Silva*, **Thomas Runte, Wolfgang Polifke**
Professur für Thermofluiddynamik
Technische Universität München
D-85747 Garching b. München, Germany
Email: silva@tfd.mw.tum.de

Luca Magri

Center for Turbulence Research
Stanford University
Stanford, California 94305-3024, U.S.A.

Cambridge University Engineering Department
Trumpington Street, Cambridge, CB2 1PZ, U.K.

ABSTRACT

Thermoacoustic instabilities are often calculated with Helmholtz solvers combined with a low-order model for the flame dynamics. Typically, such a formulation leads to an eigenvalue problem in which the eigenvalue appears under nonlinear terms, such as exponentials related to the time delays that result from the flame model. The objective of the present paper is to quantify uncertainties in thermoacoustic stability analysis with a Helmholtz solver and its adjoint. This approach is applied to the model of a combustion test rig with a premixed swirl burner. The nonlinear eigenvalue problem and its adjoint are solved by an in-house adjoint Helmholtz solver, based on an axisymmetric finite volume discretization. In addition to first-order correction terms of the adjoint formulation, as they are often used in literature, second-order terms are also taken into account. It is found that one particular second-order term has significant impact on the accuracy of the predictions. Finally, the Probability Density Function of the growth rate in the presence of uncertainties in the input parameters is calculated with a Monte Carlo approach. The uncertainties considered concern the gain and phase of the flame response, the outlet acoustic reflection coefficient, and the plenum geometry. It is found that the second-order adjoint method gives quantitative agreement with results based on the full nonlinear eigenvalue problem, while requiring much fewer computations.

NOMENCLATURE

Abbreviations:

DR	Damping rate
FTF	Flame Transfer Function
PDF	Probability Density Function

Greek:

α	Plenum cone angle
$\delta\eta$	Parameter perturbation
$\delta\omega$	Actual perturbed eigenfrequency
$\delta\sigma$	Actual eigenvalue perturbation (drift)
$\delta\tilde{\sigma}$	Prediction on eigenvalue perturbation (drift) by adjoint methods
η	Generic set of thermoacoustic parameters
ω	Complex eigenfrequency, $\omega^r + i\omega^i$
ω^i	Growth rate
ω^r	Angular frequency
ϕ	Phase in the flame model
σ	Complex eigenvalue, $\sigma = -\omega^2$
τ	Flame time delay
$\tilde{\omega}$	Perturbed eigenfrequency calculated by adjoint methods
$\tilde{\sigma}$	Perturbed eigenvalue calculated by adjoint methods
φ	Argument of R_{out}, $\varphi = \arg(R_{out})$

*Address all correspondence to this author.

Mathematical:

$\mathscr{A}$	Helmholtz equation divergence operator
$\mathscr{B}$	Acoustic boundary condition operator
$\mathscr{F}$	Flame Transfer Function (FTF)
$\mathscr{H}$	Heat release rate operator
$\mathscr{L}$	Operator, $\mathscr{L} = \mathscr{A} - \mathscr{H} + \mathscr{B}$
$\mathscr{N}$	Helmholtz eigenvalue problem operator, $\mathscr{N} = \mathscr{L} - I\sigma$

Roman:

$\delta\hat{p}$	Acoustic pressure perturbation
$\hat{q}$	Fourier transform of heat release rate
$\hat{p}$	Fourier transform of acoustic pressure (eigenvector)
$\hat{p}^\dagger$	Adjoint pressure eigenvector
i	Imaginary unit, $\mathrm{i}^2 + 1 = 0$
G	Flame gain
I	Identity operator
l_1	Plenum longitudinal length
R_{out}	Outlet acoustic reflection coefficient
$T1\mathrm{ord}$	First-order term in adjoint Taylor expansion
$T2\mathrm{ord}$	Second-order term in adjoint Taylor expansion

Subscripts:

0	Reference (unperturbed) variable
1	First-order perturbation (correction)
2	Second-order perturbation (correction)

Superscripts:

$*$	Complex conjugate
Fm	Flame model
Ge	Geometry
H	Conjugate transpose
Rm	Reflection coefficient model

INTRODUCTION

Thermoacoustic instabilities in combustion systems originate from the two-way interaction between the flame dynamics and the acoustic environment. In spite of the considerable attention that has been given to thermoacoustic instabilities by the combustion community for several decades, this type of instability remains highly unpredictable and it generally is detected only at the later stages of development, when the full combustor is tested [1]. It is therefore essential to develop methodologies to predict thermoacoustic instabilities at the early stages of design. A robust, reliable approach should include strategies to estimate the uncertainty of model predictions, which are introduced, among others, by the uncertainties in model and design parameters [2].

Helmholtz solvers coupled with models for the flame dynamics have demonstrated their capability to predict thermoacoustic instabilities in low-Mach number combustion systems with complex geometries [3]. These numerical tools solve a nonlinear eigenvalue problem to estimate both the thermoacoustic mode structure and the corresponding complex-valued eigenfrequency, which corresponds to the resonance frequency and the growth rate of the corresponding thermoacoustic mode. In fully premixed combustion, the unsteady heat release rate of the flame is well-correlated to upstream velocity perturbations. In this case, the effects of flame dynamics are included by coupling a Helmholtz solver with a suitable Flame Transfer Function (FTF). Recent studies have also demonstrated the potential of this hybrid approach to evaluate limit cycle amplitudes when used in combination with a Flame Describing Function [4, 5].

However, there is only a small number of methodologies proposed in the literature to perform Uncertainty Quantification (UQ) of thermoacoustic instabilities when considering Helmholtz solvers [6]. UQ may be crucial in cases where input design parameters contain a certain degree of uncertainty around a given mean value. Examples of such uncertainties are manufacturing tolerances or noise in input measurements, which in turn can introduce uncertainty in the geometry of the system, the acoustic impedance at a given boundary, or the values of the gain and phase of the FTF.

UQ studies can be carried out by performing Monte Carlo simulations, in which it is typically necessary to consider thousands of realizations. In each realization, one nonlinear eigenvalue problem is to be solved for a given combination of *perturbed* input parameters, i.e., input parameter values drawn from a presumed Probability Density Function (PDF). For each realization the (complex-valued) eigenfrequency of the perturbed problem is determined. The deviation of the latter with respect to the corresponding unperturbed value is called 'eigenfrequency drift'. After thousands of realizations, the PDF of the perturbed eigenfrequency can be evaluated. In so doing, it is possible to determine (i) the most probable frequency and growth rate of instability and (ii) the corresponding margins of reliability in the presence of uncertainty.

In order to decrease the computational costs required to construct an accurate PDF, surrogate models for the eigenfrequency, which are algebraic expressions obtained by regression, may be used instead of the full Helmholtz equation [6]. Additionally, surrogate models can be combined with Active Subspace techniques so that the number of uncertain input parameters is reduced [7]. By doing so, the cost of carrying out Monte Carlo simulations can be reduced. Of course, the accuracy of the results strongly depends on the quality of the surrogate model.

In this work, a novel approach is used to build such a surrogate model. Instead of a linear combination of selected input parameters, an adjoint formulation, derived from the nonlinear eigenvalue problem, is used to estimate the eigenfrequency drift of a given thermoacoustic mode. This approach is based on a second-order Taylor expansion of the eigenvalue problem around the unperturbed conditions. The formulation obtained is greatly

simplified when exploiting some mathematical properties of the so-called adjoint eigenmodes [8–10]. One of the main advantages of this approach is that the eigenfrequency drift is well-estimated at low computational cost. Further advantages are of interest to computational fluid dynamics. For example, instead of considering input design parameters to be individual scalar values (such as global gain and time delay in simplified flame models or a length of a given duct in a simplified geometry), adjoint analysis considers input design parameters to be also scalar fields. That is why, for example, the eigenvalue drift due to a small local change of two or three dimensional flames/flows can be computed [11, 12].

Adjoint methods, as applied to classic flow instability and eigenvalue sensitivity, help calculate (i) the forced response (receptivity) of the flow to external forcing and (ii) the sensitivity of eigenvalues to perturbations of the flow. These perturbations can be caused by external objects placed in the flow or generic changes in the equations' structure, for example by varying a parameter, such as the Reynolds number. In all likelihood, Tumin and Fedorov [13] and Hill [14] were the first to apply adjoint techniques to hydrodynamics, in particular, to boundary-layer instability and the flow past a cylinder, respectively. The above studies inspired many other applications in hydrodynamic stability, as recently reviewed by Luchini and Bottaro [12].

In thermoacoustics, first-order methods of linear eigenproblems were developed and proposed by Magri and Juniper [15]. Adjoint methods, as applied to eigenvalue sensitivity, were first developed and applied to a Rijke-tube configuration with an n-τ model by Magri et al. [9, 16] to find the optimal passive mechanisms and base-state changes to stabilize the system. This method was applied to a ducted diffusion flame modeled by the mixture fraction in [11]. This was achieved by analyzing the eigenvalue drift predicted by a compact mathematical expression involving the direct and adjoint thermoacoustic eigenvectors of interest, and the system perturbation matrix. However, the stability of most thermoacoustic systems is governed by nonlinear eigenproblems, i.e., the eigenvalue appears under nonlinear terms. The theoretical extension of thermoacoustic adjoint sensitivity analysis to nonlinear eigenproblems was proposed by Magri [8] and Juniper et al. [10]. The first application of this theory to uncertainty quantification of an annular combustor was discussed in the doctoral thesis of Magri [8]. Mensah and Moeck [17] applied first-order adjoint methods and Bloch-wave theory to calculate efficiently the thermoacoustic-mode change in an annular combustor due to symmetry breaking.

The present paper applies the above adjoint sensitivity methods for the first time to a combustion test rig with a premixed swirl burner, the thermoacoustic stability of which is governed by an inhomogeneous Helmholtz equation in a fairly elaborated computational domain. The resulting *nonlinear* eigenvalue problem requires the calculation of first- and second-order eigenvalue corrections for accurate uncertainty quantification of thermoacoustic stability via a Monte Carlo method.

This article is organized as follows. In the next section a brief description of the combustor under study is provided. Subsequently, the nonlinear eigenvalue problem is derived from the Helmholtz equation assuming a model for the flame dynamics and acoustic boundary conditions. In the fourth section, the expression for the eigenfrequency drift is derived by adjoint analysis. In the fifth section, some results are shown to validate the procedure in terms of eigenfrequency drift estimation. Finally, two configurations are studied to obtain the PDF of the growth rates of the first thermoacoustic mode via a combination of a Monte Carlo method with the adjoint formulation. It is shown that, although the reference growth rate for both configurations is the same, the probabilities that the configurations are unstable are different. The technique proposed in this study can help accurately predict the probability that a combustion system exhibits is unstable with affordable computational effort.

SWIRLED COMBUSTOR

The turbulent swirled combustor under investigation, designed and built at EM2C laboratory, has been widely studied in the context of combustion instabilities [4, 18, 19]. This axisymmetric combustor, as illustrated in Fig. 1, consists of a cylindrical plenum of variable length l_1, a convergent duct in which a swirler induces a flow with swirl number of 0.55, and a cylindrical combustion chamber of variable length l_3. Here, the length is fixed to $l_3 = 0.4$ m. A mixture of methane and air at an equivalence ratio of 0.8 is injected upstream of the plenum. The operating condition 'B' of Palies et al. [19] and Silva et al. [4] is considered in this study. The corresponding flame has a total power of $\bar{\dot{Q}} = 3.03$ kW with a mean flow velocity at the reference position of $\bar{u}_{\text{ref}} = 4.16$ ms^{-1}.

SWIRLED COMBUSTOR THERMOACOUSTIC MODEL

By using modal transformations for the acoustic pressure, $p(\mathbf{x},t) = \hat{p}(\mathbf{x})\exp(-\mathrm{i}\omega t)$, and heat release rate, $\dot{q}(\mathbf{x},t) = \hat{\dot{q}}(\mathbf{x})\exp(-\mathrm{i}\omega t)$, the thermoacoustic stability of the low-Mach number combustion system under investigation is governed by the inhomogeneous Helmholtz equation

$$\nabla\cdot\left(\bar{c}^2\nabla\hat{p}\right) + \omega^2\hat{p} = \mathrm{i}\omega(\gamma-1)\hat{\dot{q}}(\mathbf{x}), \tag{1}$$

where p, $\dot{q}$, c and γ denote the pressure, local heat release rate, mean-flow speed of sound and specific heat ratio, respectively. For brevity, the spatial dependency of $\hat{p}$ is dropped. In addition, ω denotes the complex eigenfrequency, i is the imaginary unit, the overbar $\bar{}$ is the temporal mean and the hat $\hat{}$ represents the Fourier transform. In general, the *local* Flame Transfer Function

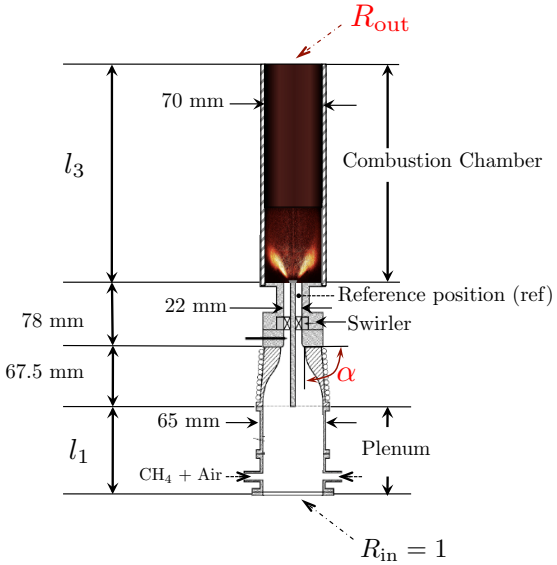

FIGURE 1. Turbulent swirled combustor configuration under investigation. Adapted from Palies et al. [18]

(FTF) is defined as

$$\mathscr{F}(\mathbf{x},\omega)_{\text{loc}} = G_{\text{loc}}(\mathbf{x},\omega)e^{\mathrm{i}\phi_{\text{loc}}(\mathbf{x},\omega)} = \frac{\hat{q}(\mathbf{x})/\bar{q}(\mathbf{x})}{\hat{\mathbf{u}}\cdot\mathbf{n}_{\text{ref}}/\bar{u}_{\text{ref}}}, \tag{2}$$

where G_{loc} and ϕ_{loc} are the spatially varying gain and phase, respectively. In addition, u, $\mathbf{n}$ and $[]_{\text{ref}}$ are the velocity, the normal vector aligned with the longitudinal axis of the combustor, and the value of a given quantity at the reference position, respectively. Considering that from the momentum conservation $\hat{u}_{\text{ref}} = \nabla\hat{p}_{\text{ref}}/(\mathrm{i}\omega\bar{\rho})$, where $\bar{\rho}$ is the mean-flow density, and substituting Eqn. (2) into Eqn. (1) for $\hat{q}(\mathbf{x})$, the Helmholtz equation becomes

$$\underbrace{\nabla\cdot\left(\bar{c}^2\nabla\hat{p}\right)}_{\mathscr{A}\hat{p}} + \underbrace{\omega^2\hat{p}}_{\omega^2\hat{p}} - \underbrace{(\gamma-1)\frac{\bar{q}\nabla\hat{p}_{\text{ref}}\cdot\mathbf{n}_{\text{ref}}}{\bar{\rho}\bar{u}_{\text{ref}}}G_{\text{loc}}(\mathbf{x},\omega)e^{\mathrm{i}\phi_{\text{loc}}(\mathbf{x},\omega)}}_{\mathscr{H}(\omega)\hat{p}} = 0. \tag{3}$$

This equation is equipped with Robin boundary conditions

$$\underbrace{\nabla\hat{p}+\beta\hat{p}}_{\mathscr{B}(\omega)\hat{p}} = 0, \quad \text{where} \quad \beta = \mathrm{i}\frac{\omega}{\bar{c}}\frac{(1-R(\omega))}{(1+R(\omega))}, \tag{4}$$

and R is the frequency-dependent reflection coefficient at a given boundary.

First, we assume that the flame gain, G_{loc}, and phase, ϕ_{loc}, are constant within the flame region and zero elsewhere. By choosing $\bar{q} = \bar{\dot{Q}}/V_f$, where $\dot{Q}$ is the global heat release rate and V_f denotes the volume of the flame region, we relabel $G_{\text{loc}} = G$ and $\phi_{\text{loc}} = \phi$ and interpret them as the gain and phase of a measured *global* FTF, as suggested by Silva et al. [4]. It was also shown that the influence of the flame spatial distribution on the eigenfrequency prediction is negligible in compact flames [4], such as the one under investigation. Second, we assume the gain G is independent of frequency, while the phase is modeled as $\phi = \omega\tau$, where τ is a constant characteristic time delay of the flame response. This assumption holds in a range close to a reference frequency [20]. Here, the reference frequency is that of the first thermoacoustic mode. For more versatility and accuracy, the dependency on the frequency should be included using impulse responses, experimental FTFs, etc. Although this is beyond the scope of the present work, the methods presented in this paper can readily accommodate such a frequency dependency with little modification of the algorithm.

Defining the eigenvalue $\sigma = -\omega^2$ for brevity, the nonlinear eigenvalue problem, which arises from Eqns. (3)-(4), reads

$$\underbrace{[\mathscr{A} - \mathscr{H}(\sigma) + \mathscr{B}(\sigma)]}_{\mathscr{L}}\hat{p} = \sigma\hat{p}, \tag{5}$$

where $\hat{p}$ is an eigenvector representing a given eigenmode of the thermoacoustic system. Solving the eigenvalue problem of Eqn. (5) means finding simultaneously the values of σ and $\hat{p}$ that satisfy Eqn. (5). It should be noted that for a passive flame, where $G = 0$ and therefore $\mathscr{H} = 0$, and for open ($\mathscr{B}\hat{p} = \hat{p}$) or closed ($\mathscr{B}\hat{p} = \nabla\hat{p}$) acoustic boundary conditions, the eigenvalue problem becomes linear in σ.

ADJOINT SENSITIVITY ANALYSIS

The eigenvalue problem $\mathscr{L}\hat{p} = \sigma\hat{p}$ in Eqn. (5) can be rewritten in compact form as

$$\mathscr{N}(\sigma)\,\hat{p} = 0, \tag{6}$$

where $\mathscr{N}(\sigma) = \mathscr{L} - I\sigma$ represents the (non-homogeneous) Helmholtz operator. Therefore, the operator $\mathscr{N}$ depends on the system's geometry $\mathscr{A}$, the description of the flame dynamics $\mathscr{H}$ and the boundary conditions $\mathscr{B}$. An illustration of these operators after discretization is given in Appendix A. We introduce a parameter η, which can be related to the gain of the FTF, a reflection coefficient R at a given boundary, or a given parameter of the system geometry. Hence, the problem of interest is written

Journal of Engineering for Gas Turbines and Power. Received June 17, 2016;
Accepted manuscript posted July 20, 2016. doi:10.1115/1.4034203

as

$$\mathscr{N}(\sigma_0,\eta_0)\;\hat{p}_0=0, \tag{7}$$

where the subscript '0' denotes a reference set of parameters at which the eigenvalue problem is solved, i.e., the unperturbed problem. In the following, we are interested in obtaining the solution of the eigenvalue problem (σ and $\hat{p}$) for a condition in which one or more reference parameters are slightly perturbed. Therefore, we consider a perturbed parameter $\eta=\eta_0+\delta\eta$ and, correspondingly, we expect changes in the eigenvalue σ_0 by $\delta\sigma$ and in the eigenvector $\hat{p}_0$ by $\delta\hat{p}$. The perturbed eigenvalue problem around a base solution '0' reads

$$\mathscr{N}(\sigma,\eta)\;\hat{p}=\mathscr{N}(\sigma_0+\delta\sigma,\eta_0+\delta\eta)\;(\hat{p}_0+\delta\hat{p})=0. \tag{8}$$

Instead of solving an eigenvalue problem for Eqn. (8) to obtain accurate values for σ and $\hat{p}$, we rely on the already-known solution σ_0 and $\hat{p}_0$ to estimate the values of σ and $\hat{p}$. It is shown in the following sections that, by using the adjoint method proposed, computations to obtain σ and $\hat{p}$ can be sped up by a factor of 10 (or more) with respect to the computations needed when solving for the nonlinear eigenvalue problem (8). By means of adjoint analysis, which is described in detail in Appendix B, we approximate the perturbed eigenvalue σ by $\tilde{\sigma}=\sigma_0+\delta\tilde{\sigma}$, where $\delta\tilde{\sigma}=\sigma_1+\sigma_2$ is an approximation of the actual drift $\delta\sigma$. σ_1 and σ_2 are the first- and second-order correction terms, respectively, around the unperturbed eigenvalue σ_0, therefore $|\sigma_2|\ll|\sigma_1|$ for small perturbations. In line with Magri [8] and Juniper et al. [10], they read

$$\sigma_1=\underbrace{-\frac{\eta_1\left(\hat{p}_0^{\dagger}\right)^H\left.\frac{\partial\mathscr{N}}{\partial\eta}\right|_0\hat{p}_0}{\left(\hat{p}_0^{\dagger}\right)^H\left.\frac{\partial\mathscr{N}}{\partial\sigma}\right|_0\hat{p}_0}}_{T1\text{ord}}, \tag{9}$$

$$\begin{aligned}\sigma_2\approx&\underbrace{-\frac{\sigma_1\left(\hat{p}_0^{+}\right)^H\left.\frac{\partial\mathscr{N}}{\partial\sigma}\right|_0\hat{p}_1}{\left(\hat{p}_0^{+}\right)^H\left.\frac{\partial\mathscr{N}}{\partial\sigma}\right|_0\hat{p}_0}}_{T2\text{ord}(1)}\underbrace{-\frac{\eta_1\left(\hat{p}_0^{+}\right)^H\left.\frac{\partial\mathscr{N}}{\partial\eta}\right|_0\hat{p}_1}{\left(\hat{p}_0^{+}\right)^H\left.\frac{\partial\mathscr{N}}{\partial\sigma}\right|_0\hat{p}_0}}_{T2\text{ord}(2)}\\&\underbrace{-\frac{1}{2}\frac{\sigma_1^2\left(\hat{p}_0^{+}\right)^H\left.\frac{\partial^2\mathscr{N}}{\partial\sigma^2}\right|_0\hat{p}_0}{\left(\hat{p}_0^{+}\right)^H\left.\frac{\partial\mathscr{N}}{\partial\sigma}\right|_0\hat{p}_0}}_{T2\text{ord}(3)}\underbrace{-\frac{\sigma_1\eta_1\left(\hat{p}_0^{+}\right)^H\left.\frac{\partial^2\mathscr{N}}{\partial\sigma\partial\eta}\right|_0\hat{p}_0}{\left(\hat{p}_0^{+}\right)^H\left.\frac{\partial\mathscr{N}}{\partial\sigma}\right|_0\hat{p}_0}}_{T2\text{ord}(4)},\end{aligned} \tag{10}$$

where ^{H} denotes the conjugate transpose and $\hat{p}_0^{\dagger}$ is the adjoint eigenvector of the thermoacoustic system that satisfies

$$\mathscr{L}^H\hat{p}_0^{\dagger}=\sigma^*\hat{p}_0^{\dagger}, \tag{11}$$

where * is the complex conjugate. A brief explanation of the calculation of $\hat{p}^{\dagger}$ is provided in Appendix C. Note that in Eqn. (10), the term $T2\text{ord}(5)$ (see Eqn. (31)) is neglected because its contribution is minimal, as shown in the next section. In contrast, the term $T2\text{ord}(2)$ has a large contribution to σ_2. Recalling that $\sigma=-\omega^2$, yields

$$\delta\sigma=-\left.\frac{d\omega^2}{d\omega}\right|_{\omega_0}\delta\omega=-2\omega_0\delta\omega, \tag{12}$$

and therefore we approximate the perturbed eigenfrequency ω by

$$\omega\approx\tilde{\omega}=\omega_0+\delta\tilde{\omega}=\omega_0-\frac{1}{2}\frac{\delta\tilde{\sigma}}{\omega_0}, \tag{13}$$

where $\omega_0=\sqrt{-\sigma_0}$. The solution $\omega_0=-\sqrt{-\sigma_0}$ leads to an eigenfrequency with negative frequency, which is not considered because it is unphysical. In the limit of linear eigenvalue problems, the first- and second-order correction terms σ_1 and σ_2 reduce to

$$\sigma_1=\frac{\eta_1\left(\hat{p}_0^{+}\right)^H\left.\frac{\partial\mathscr{N}}{\partial\eta}\right|_0\hat{p}_0}{\left(\hat{p}_0^{+}\right)^H\hat{p}_0}, \tag{14}$$

and

$$\sigma_2=-\frac{\sigma_1\left(\hat{p}_0^{+}\right)^H\hat{p}_1}{\left(\hat{p}_0^{+}\right)^H\hat{p}_0}+\frac{\eta_1\left(\hat{p}_0^{+}\right)^H\left.\frac{\partial\mathscr{N}}{\partial\eta}\right|_0\hat{p}_1}{\left(\hat{p}_0^{+}\right)^H\hat{p}_0}, \tag{15}$$

because $\frac{\partial\mathscr{N}}{\partial\sigma}=-I$.

RESULTS AND DISCUSSION

In the first part of this section, the eigenfrequency of the unperturbed problem ω_0 is obtained by solving the nonlinear eigenvalue problem for a given set of parameters η_0 (Eqn. (7)), characterizing the turbulent swirled combustor at a reference condition. Subsequently, a small perturbation is introduced in the geometry ($\eta=\eta_0+\delta\eta^{\text{Ge}}$), in the flame model ($\eta=\eta_0+\delta\eta^{\text{Fm}}$)

Journal of Engineering for Gas Turbines and Power. Received June 17, 2016;
Accepted manuscript posted July 20, 2016. doi:10.1115/1.4034203

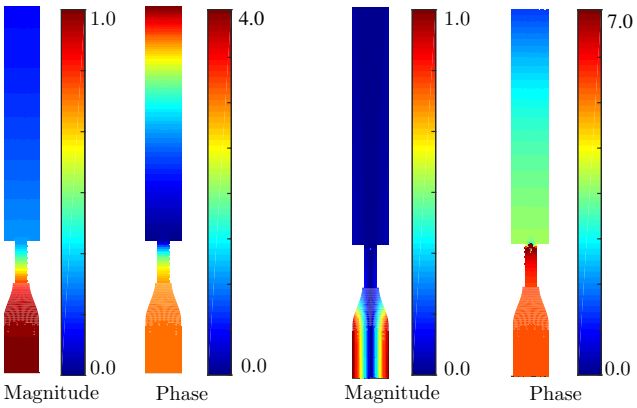

FIGURE 2. First thermoacoustic mode at $\omega_0 = (2\pi \cdot 148 + i110)$ rad.s^{-1}. (a) Direct mode, $\hat{p}_0$, and (b) adjoint mode, $\hat{p}_0^\dagger$

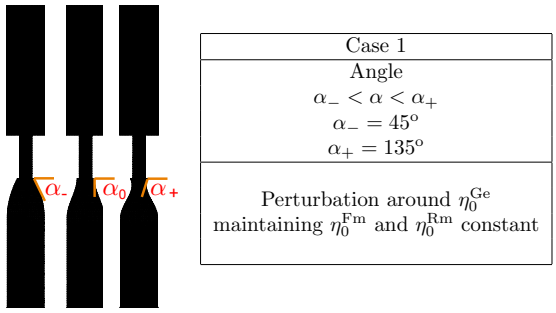

FIGURE 3. The geometrical parameter η_0^{Ge} is the plenum cone angle, α

and in the model that describes the acoustic reflection at the outlet ($\eta = \eta_0 + \delta\eta^{Rm}$). The estimated perturbed eigenfrequency $\tilde{\omega}$ is then computed by means of Eqns. (9), (10) and (13) and compared with the actual perturbed eigenfrequency ω, which is obtained by solving the full Helmholtz equation with the perturbed parameters (Eqn. (8)). Monte Carlo simulations are then performed considering simultaneous random perturbations to the flame parameters and outlet reflection coefficient, $\delta\eta^{Fm}$ and $\delta\eta^{Rm}$, around η_0, to evaluate the probability distribution and risk factor of the first thermoacoustic-mode growth rate.

The reference operating point

An in-house Helmholtz solver, which is based on a finite volume approach for axisymmetric configurations, is used to solve the nonlinear eigenvalue problem formulated in Eqn. (5) at a reference condition defined by the set of parameters η_0 illustrated in Tab. 1. A validation of the solver against experimental data and benchmark numerical solutions is shown in Appendix D. The flame (η_0^{Fm}) is modeled by a gain G_0 and time delay τ_0, which are characteristic of flame B for the frequencies of interest. The same values were considered in Ndiaye et al. [6]. In addition, a plenum length $l_1 = 0.096$ m is considered (see Fig. 1), which is used in the configuration C4 in [4]. The eigenfrequency ω is expressed as $\omega = \omega^r + i\omega^i$, where ω^r and ω^i are the real and imaginary parts, respectively. Because of the modal transformation used, ω^r is the resonance frequency, $\omega^r = 2\pi f$, and ω^i is the growth rate of the thermoacoustic mode.

Figure 2(a) shows the modulus and phase of the first longitudinal thermoacoustic mode of the turbulent swirled combustor under study, which corresponds to the eigenfrequency $\omega_0 = (2\pi \cdot 148 + i110)$ s^{-1}. The corresponding adjoint thermoacoustic mode is illustrated in Fig. 2(b), which is obtained by solving Eqn. (11) with the unperturbed parameters. In this study, this adjoint thermoacoustic mode is used to compute the values of σ_1 and σ_2. Although not pursued in this work, adjoint eigenmodes can be further exploited to carry out receptivity studies for open-loop forcing and structural sensitivity analysis [11]. The latter reveals which type of feedback mechanism may be the more effective in changing the frequency and growth rate of the system, which is relevant to combustion instability control.

TABLE 1. Reference (unperturbed) geometric parameter, η_0^{Ge}, flame model parameters, η_0^{Fm}, and outlet reflection coefficient, η_0^{Rm}, of the turbulent swirled combustor

η_0^{Ge}	η_0^{Fm} $\mathcal{F}(\omega) = G_0 e^{i\omega\tau_0}$		η_0^{Rm} $R_{out} = r_0 e^{i\varphi_0}$	
α_0	G_0	τ_0	r_0	φ_0
90°	1.0	4.73 ms	0.6	π

Eigenfrequencies of the perturbed system

Once the reference (unperturbed) solution, denoted by the subscript 0, is computed, the parameters that define the system are perturbed in an interval $\eta_- < \eta < \eta_+$ as shown in Fig. 3 and Tab. 2. Consequently, it is expected that the eigenmode $\hat{p}$ and the corresponding eigenfrequency ω of the thermoacoustic system are perturbed and drift away from $\hat{p}_0$ and ω_0, respectively. In this work, we are interested in approximating the drift $\delta\omega$ by $\delta\tilde{\omega}$, where $\delta\tilde{\omega} = \delta\tilde{\sigma}/(2\omega_0)$ and $\delta\tilde{\sigma} = \sigma_1 + \sigma_2$ (see Eqn. (13)).

Four different strategies are considered and summarized in Tab. 3. Method 0, referred to as the 'truth', consists of solving the Helmholtz equation for the perturbed parameters. In Method 1, we assume that the nonlinearity in the eigenvalue problem, which is introduced by the active flame and the Robin-type out-

Journal of Engineering for Gas Turbines and Power. Received June 17, 2016;
Accepted manuscript posted July 20, 2016. doi:10.1115/1.4034203

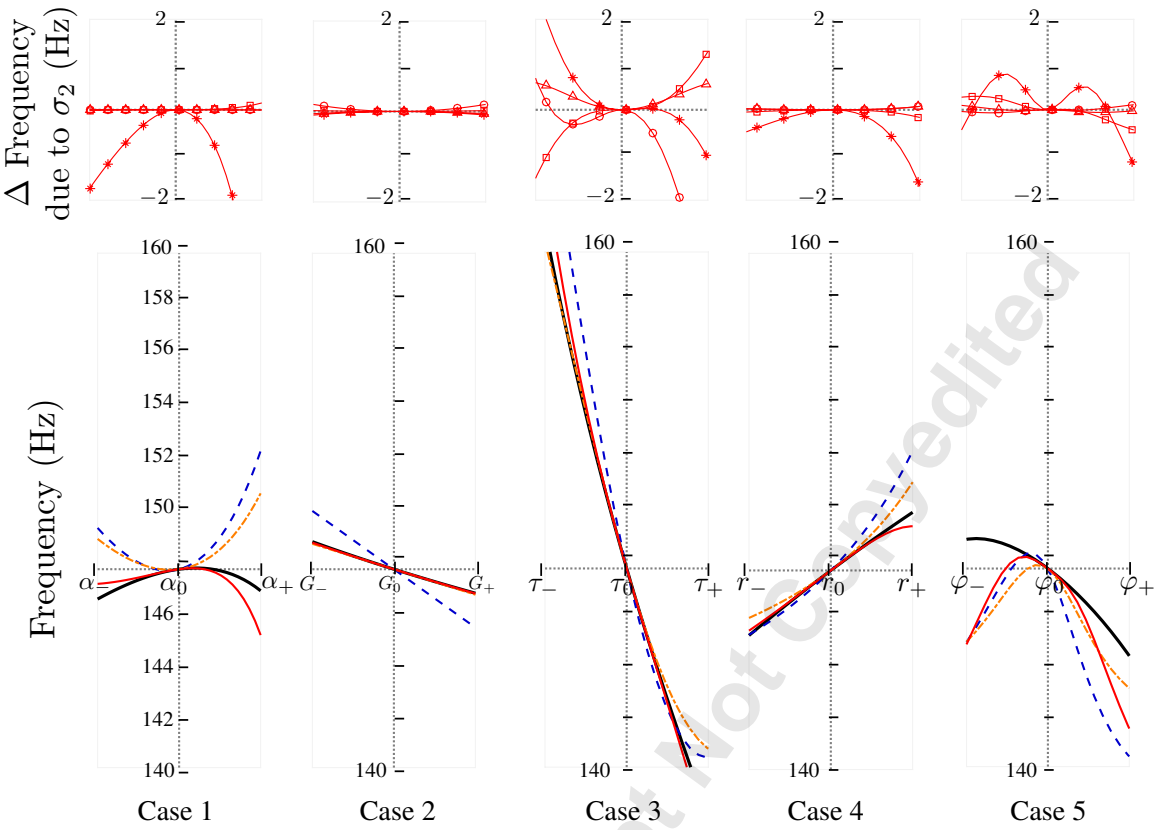

FIGURE 4. Frequency drift around the reference angular frequency, $\omega_0^r = 2\pi \cdot 148$ rad.s^{-1}, due to perturbations to the system's parameters, η_0, reported in Tab. 1. Top frames: Real $\left\{\frac{1}{2}\frac{\sigma_2}{\omega_0}\right\}/2\pi$, where $\sigma_2 = T2\text{ord}(1)$ □, $\sigma_2 = T2\text{ord}(2)$ ∗, $\sigma_2 = T2\text{ord}(3)$ △, $\sigma_2 = T2\text{ord}(4)$ ○. Bottom frames: Method 0 ——, Method 1 - -, Method 2 - -, Method 3 ——, explained in Tab. 3

TABLE 2. Perturbation ranges around the reference set of parameters η_0. Case 1 is illustrated in Fig. 3.

Case 2	Case 3	Case 4	Case 5
$\mathscr{F}(\omega)$		R_{out}	
$Ge^{i\omega\tau_0}$	$G_0 e^{i\omega\tau}$	$re^{i\varphi_0}$	$r_0 e^{i\varphi}$
$G_- < G < G_+$	$\tau_- < \tau < \tau_+$	$r_- < r < r_+$	$\varphi_- < \varphi < \varphi_+$
$G_- = 0.8$	$\tau_- = 0.8\tau_0$	$r_- = 0.8r_0$	$\varphi_- = 0.8\pi$
$G_+ = 1.2$	$\tau_+ = 1.2\tau_0$	$r_+ = 1.2r_0$	$\varphi_+ = 1.2\pi$
Perturbation around η_0^{Fm} fixing η_0^{Ge} and η_0^{Rm}		Perturbation around η_0^{Rm} fixing η_0^{Ge} and η_0^{Fm}	

let boundary condition, is negligible and therefore we consider $\frac{\partial \mathscr{N}}{\partial \sigma} = -I$. In addition, we assume that the perturbation in the eigenvector $\hat{p}_1$ is very small and therefore $\sigma_2 = 0$. The remaining expression (Eqn. (14)) is the classical formulation for computing the eigenvalue drift in systems described by a linear eigenvalue problem [16]. In Method 2, we account for the nonlinearity of the eigenvalue problem with a first-order approximation but we still consider $\sigma_2 = 0$. In Method 3 we account for the nonlinearity of the eigenvalue problem with first- and second-order approximation terms. The derivatives of the terms of Eqns. (9), (10) and (14) are computed by finite differences as explained in Appendix A.

Figures 4 and 5 (bottom frames) show the results for the five cases listed in Fig. 3 and Tab. 2Ḃy inspection, the resonance frequency and growth rate of the first thermoacoustic mode ω^r is very sensitive to changes in the time delay τ of the flame model. Interestingly, a small change in the phase φ of the outlet reflection coefficient produces a strong change in the growth rate ω^i of the first thermoacoustic mode. Two main remarks can be made concerning the formulations considered for the estimation of ω. On the one hand, it is observed that, between Methods 1-3, Method 3 (red continuous line) is the one that produces bet-

Journal of Engineering for Gas Turbines and Power. Received June 17, 2016;
Accepted manuscript posted July 20, 2016. doi:10.1115/1.4034203

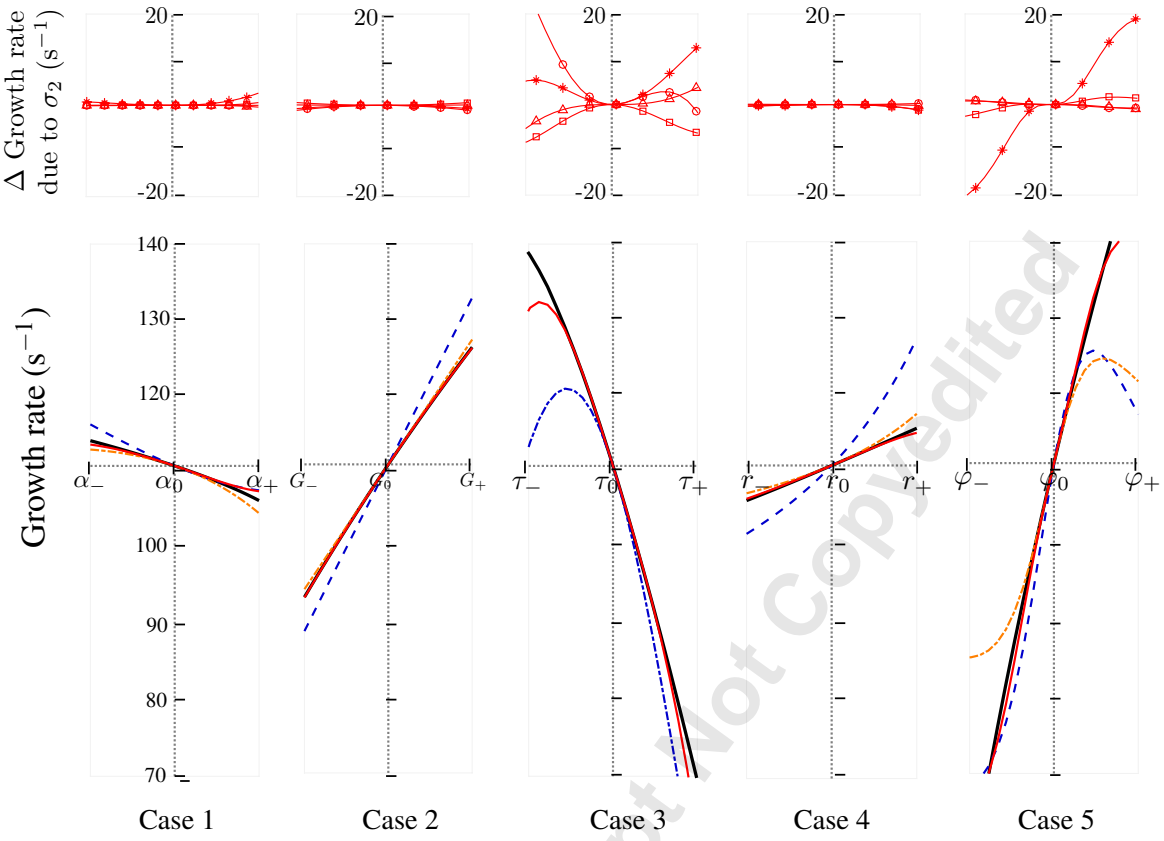

FIGURE 5. Growth-rate drift around the reference growth rate, $\omega_0^r = 2\pi \cdot 148$, rad.s^{-1}, due to perturbations to the system's parameters, η_0, reported in Tab. 1. Top frames: Imag $\left\{\frac{1}{2}\frac{\sigma_2}{\omega_0}\right\}$, where $\sigma_2 = T2\text{ord}(1)$ □, $\sigma_2 = T2\text{ord}(2)$ ∗, $\sigma_2 = T2\text{ord}(3)$ △, $\sigma_2 = T2\text{ord}(4)$ ○. Bottom frames: Method 0 ——, Method 1 - - -, Method 2 - -, Method 3 ——, explained in Tab. 3

TABLE 3. Methods used to calculate the perturbed eigenvalue

Method	Output	Equation to solve
Method 0 (Truth)	σ	Eqn. (8)
Method 1	$\tilde{\sigma} = \sigma_0 + \sigma_1$	Eqn. (14)
Method 2	$\tilde{\sigma} = \sigma_0 + \sigma_1$	Eqn. (9)
Method 3	$\tilde{\sigma} = \sigma_0 + \sigma_1 + \sigma_2$	Eqns. (9) and (10)

ter results in all cases, since it reproduces with good accuracy the value of the eigenfrequency for the perturbed problem (black line) obtained by Method 0. On the other hand, Methods 1 and 2 are not as accurate, although they still estimate well enough the trend of the drift of the eigenfrequency, with the notable exception of case 1 (Fig. (4)). Figures 4 and 5 (top frames) show the contribution to σ_2 of the four terms $T2$ord (see Eqn. (10)). Among all four terms, the one labeled $T2$ord(2) is the most important since its contribution is significant in Case 1 (change in the geometry), Case 3 (change in the time delay τ), Case 4 (change in the magnitude of R_{out}) and Case 5 (change in the phase of R_{out}). In addition, the terms $T2$ord(1), $T2$ord(3) and $T2$ord(4) seem to equally contribute to σ in Case 3, whereas only $T2$ord(1) (among the three) gives a tangible contribution in Case 5. In all the cases studied the term $T2$ord(5) (see Eqn. (31)) is very small and is neglected, accordingly.

Monte Carlo Simulations

To quantify the Probability Density Function (PDF) of the flame parameters, several experiments should be carried out for statistical inference. To the best of the authors' knowledge, there is no available data about a systematic experimental uncertainty quantification of the flame parameters. Without evidence from experiments, we need to choose a PDF representing the uncertainty of the parameters given our knowledge about them. In statistics, it is known that the optimal distribution should be maximally noncommittal with regard to missing information [21]. In other words, the probability distribution that best represents our

(lack of) knowledge about the parameters is the one with maximal information entropy. This is known as the Principle of Maximum Entropy, which provides precise criteria for the selection of the best PDF given the knowledge of the state. In our case, we assume that the values of the parameters that are very far from the mean are very unlikely to occur. This discards all the distributions with infinite tails, such as the normal distribution. Second, we assume that the the PDF is symmetric with respect to the mean value, which discards all non-symmetric options, such as the Rayleigh distribution. Third, we assume we know the maximum and minimum values of the parameters, following Bauerheim et al. [2]. In light of this, we could choose either a beta distribution or a uniform distribution. Using the Principle of Maximum Entropy, we choose the uniform distribution for the uncertain parameters because it is the least biased possible distribution given the available information.

The applicability and reliability of the methods proposed (see Tab. 3) are examined by applying Monte Carlo simulations to find the PDF of the growth rate ω^i of the first thermoacoustic mode. Two configurations are considered. One with plenum length $l_1 = 0.096$ m (as in the previous section and denoted C4 in [4]) and another with plenum length $l_1 = 0.160$ m (configuration C8 in [4]). The parameters η^{Rm}, for r and φ, and η^{Fm}, for G and τ, are simultaneously perturbed around η_0 in the interval $0.9\eta_0 < \eta < 1.1\eta_0$, where η_0^{Rm} and η_0^{Fm} are defined in Tab. 1. The set of perturbations to η follows a uniform distribution of 10000 samples, which guarantee convergence of the final PDF.

Figure 6 shows data ensembles, i.e., data clouds, plotted in the complex plane, where each point is the eigenfrequency of one realization obtained by the four methods listed in Tab. 3. When considering Methods 1, 2 and 3, only two eigenvalue problems - to obtain $\hat{p}_0$ and $\hat{p}_0^\dagger$ - need to be solved. Subsequently, only matrix-vector multiplications are performed to obtain values for σ_1 and σ_2 (see Eqns. (9), (10) and (14)). This greatly reduces the number of computations needed when solving the Helmholtz equation. As a consequence, results from these methods are computationally obtained much faster (by a factor of $\sim$10 in this study) than those from Method 0 (truth). Between Methods 1, 2 and 3, only the last one is capable of accurately representing the data cloud obtained by the benchmark Method 0. In order to make a one-to-one comparison with respect to Method 0 (M0), the 'true' growth rate ω^i (vertical axis) is plotted against the growth rate $\tilde{\omega}^i$ calculated from Methods 1-3 (horizontal axis) in the top frames of Fig. 7, for configuration C4, and Fig. 8, for configuration C8. As expected, the growth rate obtained from Method 3 (in red) is the closest to the truth because the scattering around the straight line is small. This means that first- and second-order correction terms accounting for the eigenvalue nonlinearity are necessary to accurately predict the eigenfrequency drift, $\delta\omega$, in the presence of uncertainties.

In Silva et al. [4] and Ndiaye et al. [6], based on the experimental measurements of Palies et al. [22, 23] and by considering that the combustor responds to incoming acoustic waves as a second-order harmonic oscillator where the damping is related to the resonance sharpness, the Damping Rate (DR) of the combustor at the operating condition B was evaluated to be DR= 125 s^{-1}. A confidence interval of $\pm 10\%$ was also estimated to account, among others, for the uncertainty on the outlet reflection coefficient. Consequently, a combustion instability may take place if the growth rate of a given thermoacoustic mode exceeds the damping rate (if $\omega^i > \mathrm{DR}$). When solving the unperturbed problem for C4 and C8, it is found that $\omega_0 = 2\pi \cdot 148 + \mathrm{i}110\ \mathrm{s}^{-1}$ and $\omega_0 = 2\pi \cdot 130 + \mathrm{i}110\ \mathrm{s}^{-1}$ for both C4 and C8, respectively. Based on these results, both configurations C4 and C8 exhibit the same growth rate, and are both marginally stable. We study now which of these two systems is more likely to become thermoacoustically unstable if uncertainty in the input parameters is present. Consequently, we analyze the PDF of the growth rate for the two configurations C4 and C8, which is obtained from the data generated by Methods 0-3. It is observed from Figs. 7 and 8 that the PDF of the data generated by Method 3 (in red) agrees favorably with the one associated with Method 0 (in black). This is a further proof of the reliability of Method 3 to study uncertainty quantification with a Helmholtz. We introduce the risk factor [2], defined as

$$\text{risk factor}(\%) = \int_{\mathrm{DR}}^{\infty} \mathrm{PDF}(\omega^i)\mathrm{d}\omega^i. \tag{16}$$

Accordingly, by measuring the area of the PDF lying to the right of DR=125 s^{-1}, it is possible to estimate the probability of the occurrence of a thermoacoustic instability, given uncertainties on the inputs. Configuration C4 has a higher risk factor than configuration C8, although both have the same growth rate at the reference condition ($\omega_0 = 110\ \mathrm{s}^{-1}$).

In summary, a single deterministic computation to obtain ω_0, as often done in preliminary design, may not be sufficient to guarantee that the system is stable when uncertainties are present. Combining UQ and adjoint methods in a Helmholtz solver can improve robust stability calculation of thermoacoustic systems.

CONCLUSIONS

Sensitivity and uncertainty quantification of frequencies and growth rates of thermoacoustic modes of a turbulent swirled combustor was carried out via an adjoint Helmholtz solver. It is found that by considering an adjoint formulation that contains in addition to first-order also second-order correction terms, the eigenfrequency drift due to uncertainties in input design parameters can be estimated with quantitative accuracy. With the adjoint method, Monte Carlo Simulations can be carried out at computational cost much lower than that of the standard practice, in which Monte Carlo realizations are obtained by repeatedly solv-

Journal of Engineering for Gas Turbines and Power. Received June 17, 2016;
Accepted manuscript posted July 20, 2016. doi:10.1115/1.4034203

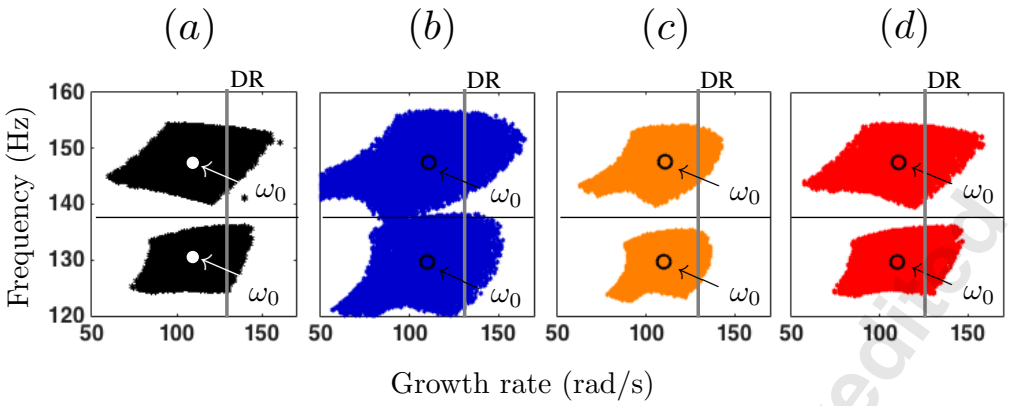

FIGURE 6. Monte Carlo simulations around the unperturbed parameters, η_0, containing 10000 realizations. Top frames: configuration C4 ($l_1 = 0.096$ m) where $\omega_0 = (2\pi \cdot 148 + \mathrm{i}110)$ s^{-1}. Bottom frames: configuration C8 ($l_1 = 0.160$ m) where $\omega_0 = (2\pi \cdot 130 + \mathrm{i}110)$ s^{-1}. The benchmark solution is given by Method 0 shown in black in column (a). The adjoint solutions are shown in column (b) Method 1 (blue), (c) Method 2 (orange), (d) Method 3 (red). A summary of the methods is reported in Tab. 3. Growth rates on the right of the vertical line (damping rate DR) are unstable

ing the full nonlinear eigenvalue problem. In the case considered in this study, it was possible to perform the uncertainty quantification about ten times faster.

For the adjoint method proposed to give accurate results, the uncertainties of the design parameters should not exceed $\sim 20\%$ of their mean values, as observed in this study. For larger perturbations/uncertainties $\gtrsim 20\%$, the second-order adjoint formulation becomes less accurate. A third-order expansion would improve the predictions, however, the complicated expressions might make the formulation too cumbersome to be practical. It is reasonable to expect that in industrial design the uncertainty on the input/design parameters, such as the flame model, does not exceed 10-20 %. Larger uncertainties may be unacceptable from a design point of view. This makes the adjoint Helmholtz solver an attractive tool for practical, fast and accurate calculation of thermoacoustic stability and its uncertainty.

ACKNOWLEDGMENT

C. F. Silva, L. Magri and W. Polifke gratefully acknowledge the 2014 Center for Turbulence Research Summer Program (Stanford University), where discussions initiated this work. L. Magri is grateful for the financial support received from "Technological foundations for the design of thermally and mechanically highly loaded components of future space transportation systems (SFB TR40)", which sponsored his visit at TU München, Germany. L. Magri also gratefully acknowledges the support from the Royal Academy of Engineering Research Fellowships Scheme.

REFERENCES

[1] Lieuwen, T., and Yang V., (Eds.), 2005. "Combustion instabilities in gas turbine engines: operational experience, fundamental mechanisms and modeling". *Prog. in Astronautics and Aeronautics AIAA,* ***210***.

[2] Bauerheim, M., Ndiaye, A., Constantine, P., Moreau, S., and Nicoud, F., 2016. "Symmetry breaking of azimuthal thermoacoustic modes: the UQ perspective". *J. Fluid Mech.,* ***789***, pp. 534–566.

[3] Nicoud, F., Benoit, L., and Sensiau, C., 2007. "Acoustic modes in combustors with complex impedances and multidimensional active flames". *AIAA Journal,* ***45***, pp. 426–441.

[4] Silva, C. F., Nicoud, F., Schuller, T., Durox, D., and Candel, S., 2013. "Combining a Helmholtz solver with the flame describing function to assess combustion instability in a premixed swirled combustor". *Combust. Flame ,* ***160***(9), pp. 1743–1754.

[5] Cuquel, A., Silva, C., Nicoud, F., Durox, D., and Schuller, T., 2013. "Prediction of the nonlinear dynamics of a multiple flame combustor by coupling the describing function methodology with a helmholtz solver". In Proceedings of ASME Turbo Expo 2013, no. GT2013-95659, ASME.

[6] Ndiaye, A., Bauerheim, M., Moreau, S., and Nicoud, F., 2015. "Uncertainty quantification of thermoacoustic instabilities in a swirled stabilized combustor". In ASME Turbo Expo 2015: Turbine Technical Conference and Exposition, no. ASME GT-2015-44133, American Society of Mechanical Engineers.

[7] Constantine, P. G., Dow, E., and Wang, Q., 2014. "Active subspace methods in theory and practice: Applications to

Journal of Engineering for Gas Turbines and Power. Received June 17, 2016;
Accepted manuscript posted July 20, 2016. doi:10.1115/1.4034203

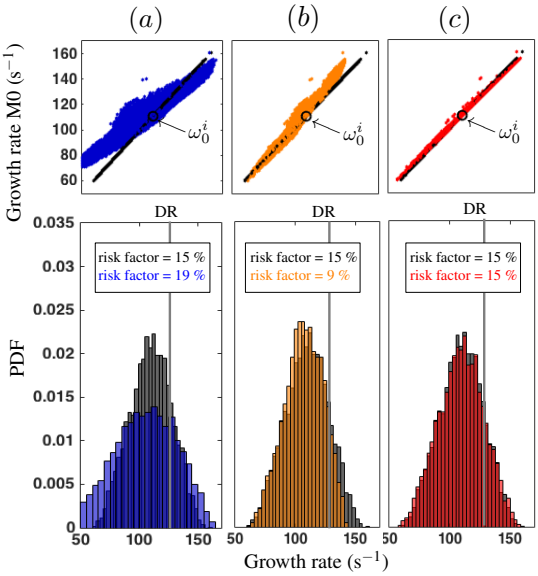

FIGURE 7. Distribution of the growth rates obtained from 10000 Monte Carlo realizations for configuration C4 ($l_1 = 0.096$ m). Top frames: distribution of the adjoint solution, $\tilde{\omega}^i$, with respect to the benchmark solution, ω^i, given by the straight line. The higher the scattering, the lower the accuracy of the adjoint solution. Bottom frames: PDF of the perturbed growth rate. In all the panels, the benchmark solution is given by Method 0 in black. The solutions obtained by the three adjoint-based methods (see Tab. 3) are reported in color in column (a) Method 1 (blue), (b) Method 2 (orange), (c) Method 3 (red). Growth rates to the right of the vertical line (damping rate DR) correspond to unstable modes

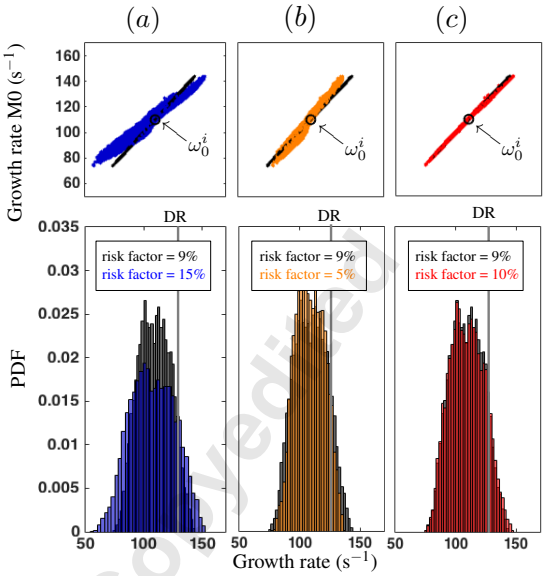

FIGURE 8. Same as Fig. 7 for configuration C8 ($l_1 = 0.160$ m)

kriging surfaces". *SIAM Journal on Scientific Computing,* ***36***(4), pp. A1500–A1524.

[8] Magri, L., 2015. "Adjoint methods in thermo-acoustic and combustion instability". PhD thesis, University of Cambridge.

[9] Magri, L., and Juniper, M. P., 2013. "A Theoretical Approach for Passive Control of Thermoacoustic Oscillations: Application to Ducted Flames". *J. Eng. Gas Turbines Power,* ***135***(9), aug, p. 091604.

[10] Juniper, M. P., Magri, L., Bauerheim, M., and Nicoud, F., 2014. "Sensitivity analysis of thermo-acoustic eigenproblems with adjoint methods". In Cent. Turbul. Res. Summer Progr., pp. 189–198.

[11] Magri, L., and Juniper, M. P., 2014. "Global modes, receptivity, and sensitivity analysis of diffusion flames coupled with duct acoustics". *J. Fluid Mech.,* ***752***, jul, pp. 237–265.

[12] Luchini, P., and Bottaro, A., 2014. "Adjoint equations in stability analysis". *Annu. Rev. Fluid Mech.,* ***46***, pp. 1–30.

[13] Tumin, A. M., and Fedorov, A. V., 1984. "Instability wave excitation by a localized vibrator in the boundary layer". *J. Appl. Mech. Tech. Phys.,* ***25***, pp. 867–873.

[14] Hill, D. C., 1992. *A theoretical approach for analyzing the restabilization of wakes*. National Aeronautics and Space Administration, Ames Research Center.

[15] Magri, L., and Juniper, M. P., 2014. "Adjoint-based linear analysis in reduced-order thermo-acoustic models". *Int. J. Spray Combust. Dyn.,* ***6***(3), pp. 225–246.

[16] Magri, L., and Juniper, M. P., 2013. "Sensitivity analysis of a time-delayed thermo-acoustic system via an adjoint-based approach". *Journal of Fluid Mechanics,* ***719***, pp. 183–202.

[17] Mensah, G. A., and Moeck, J. P., 2015. "Efficient computation of thermoacoustic modes in annular combustion chambers based on Bloch-wave theory". In ASME Turbo Expo, GT2015-43476.

[18] Palies, P., Durox, D., Schuller, T., and Candel, S., 2010. "The combined dynamics of swirler and turbulent premixed swirling flames". *Combust. Flame ,* ***157***, pp. 1698–1717.

[19] Palies, P., Durox, D., Schuller, T., and Candel, S., 2011. "Nonlinear combustion instabilities analysis based on the flame describing function applied to turbulent premixed swirling flames". *Combust. Flame ,* ***158***, pp. 1980–1991.

[20] Schmid, M., Blumenthal, R., Schulze, M., Polifke, W., and Sattelmayer, T., 2013. "Quantitative stability analysis using real frequency response data". *J. Eng. Gas Turbines Power,* ***135***(12), p. 121601.

[21] Jaynes, E. T., 1957. "Information Theory and Statistical Mechanics". *Phys. Rev.,* ***106***(4), pp. 620–630.

[22] Palies, P., 2010. "Dynamique et instabilités de combustion des flammes swirlées". PhD thesis, Ecole Centrale Paris.

[23] Palies, P., Durox, D., Schuller, T., and Candel, S., 2011. "Nonlinear combustion instability analysis based on the flame describing function applied to turbulent premixed swirling flames". *Combust. Flame,* ***158***(10), pp. 1980–1991.

[24] Runte, T., 2014. "Adjoint sensitivity analysis of a 2D FVM discretized combustor to combustion instabilities". Master's thesis, TU München.

Appendix A: Using Finite Differences to compute the derivatives of the operator $\mathscr{N}(\sigma,\eta)$ with respect to σ and η

After discretization by finite volumes of the Helmholtz equation (5), the operators $\mathscr{A}$, $\mathscr{H}$ and $\mathscr{B}$ become square matrices of size $N\times N$, where N is the number of nodes considered. In this study, numerical convergence was reached for $N>6000$. In Fig. 9 we illustrate the structures of the matrices $\mathscr{L},\mathscr{A}$, $\mathscr{H}$ and $\mathscr{B}$ at the reference condition '0'.

We consider a small perturbation η_1 in the geometry, flame model and boundary condition, as done in the second part of the section 'Results'. By doing so, the matrices $\mathscr{A}$, $\mathscr{H}$ and $\mathscr{B}$ are slightly perturbed. In order to quantify the drift in the operator $\mathscr{N}$, given a perturbation η_1, we compute

$$\eta_1 \left.\frac{\partial\mathscr{N}}{\partial\eta}\right|_0 \approx \Delta\mathscr{N}|_0 = \mathscr{N}(\sigma_0,\eta_0+\eta_1)-\mathscr{N}_0(\sigma_0,\eta_0). \quad (17)$$

Equation (17) is found in Eqns. (30) and (31) in the terms $T1ord$, $T2ord(2)$. The matrix $\Delta\mathscr{N}|_0$ is therefore the approximation of $\eta_1 \left.\frac{\partial\mathscr{N}}{\partial\eta}\right|_0$ by finite differences. In a similar way, we can compute

$$\left.\frac{\partial\mathscr{N}}{\partial\sigma}\right|_0 \approx \frac{\mathscr{N}(\sigma_*,\eta_0)-\mathscr{N}(\sigma_0,\eta_0)}{\sigma_*-\sigma_0}, \quad (18)$$

where $\sigma_* = \sigma_0 + a\sigma_0$ is a small perturbation around σ_0. In this study a is considered to be 0.01. Larger values of a deteriorate the numerical estimation of the derivative. Another term of interest can be computed as follows

$$\eta_1 \left.\frac{\partial^2\mathscr{N}}{\partial\sigma\partial\eta}\right|_0 = \eta_1\frac{\partial}{\partial\sigma}\left(\frac{\partial\mathscr{N}}{\partial\eta}\right) \approx \frac{\eta_1 \left.\frac{\partial\mathscr{N}}{\partial\eta}\right|_{\sigma_*} - \eta_1 \left.\frac{\partial\mathscr{N}}{\partial\eta}\right|_{\sigma_0}}{\sigma_*-\sigma_0}$$

$$= \frac{\mathscr{N}(\eta_0+\eta_1,\sigma_*)-\mathscr{N}(\eta_0,\sigma_*)-\mathscr{N}(\eta_0+\eta_1,\sigma_0)+\mathscr{N}(\eta_0,\sigma_0)}{\sigma_*-\sigma_0}. \quad (19)$$

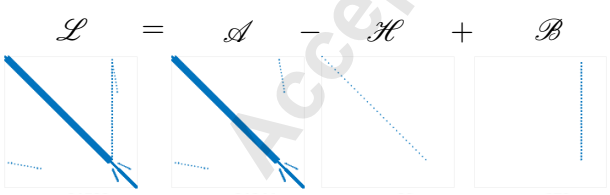

FIGURE 9. Structure of the matrices $\mathscr{L},\mathscr{A}$, $\mathscr{H}$ and $\mathscr{B}$. Blue dots represents nonzero elements

Appendix B: Adjoint analysis to obtain an approximated solution of the perturbed eigenvalue

We perform a Taylor expansion of the operator $\mathscr{N}(\sigma,\eta)$ where only first- and second-order terms are kept. Following [8, 10], it reads

$$\mathscr{N}(\sigma_0+\delta\sigma,\eta_0+\delta\eta) \approx \mathscr{N}(\sigma_0,\eta_0) + \begin{bmatrix}\delta\sigma & \delta\eta\end{bmatrix}\begin{bmatrix}\frac{\partial\mathscr{N}}{\partial\sigma}\\ \frac{\partial\mathscr{N}}{\partial\eta}\end{bmatrix}_{\sigma_0,\eta_0} + \frac{1}{2}\begin{bmatrix}\delta\sigma & \delta\eta\end{bmatrix}\begin{bmatrix}\frac{\partial^2\mathscr{N}}{\partial\sigma^2} & \frac{\partial^2\mathscr{N}}{\partial\sigma\partial\eta}\\ \frac{\partial^2\mathscr{N}}{\partial\eta\partial\sigma} & \frac{\partial^2\mathscr{N}}{\partial\eta^2}\end{bmatrix}_{\sigma_0,\eta_0}\begin{bmatrix}\delta\sigma\\ \delta\eta\end{bmatrix}. \quad (20)$$

By defining

$$\delta\sigma = \varepsilon\sigma_1+\varepsilon^2\sigma_2, \quad (21)$$
$$\delta\eta = \varepsilon\eta_1, \quad (22)$$
$$\delta\hat{p} = \varepsilon\hat{p}_1+\varepsilon^2\hat{p}_2, \quad (23)$$

where ε is a small perturbation, substituting the previous definition into Eqn. (20) and keeping only terms up to second order, yields

$$\mathscr{N}(\sigma_0+\varepsilon\sigma_1+\varepsilon^2\sigma_2,\eta_0+\varepsilon\eta_1)\,(\hat{p}_0+\varepsilon\hat{p}_1+\varepsilon^2\hat{p}_2) = A+\varepsilon B+\varepsilon^2 C, \quad (24)$$

where

$$A = \mathscr{N}(\sigma_0,\eta_0)\,\hat{p}_0, \quad (25)$$
$$B = \mathscr{N}(\sigma_0,\eta_0)\,\hat{p}_1+\sigma_1\left.\frac{\partial\mathscr{N}}{\partial\sigma}\right|_0\hat{p}_0+\eta_1\left.\frac{\partial\mathscr{N}}{\partial\eta}\right|_0\hat{p}_0, \quad (26)$$

$$C = \mathscr{N}(\sigma_0,\eta_0)\,\hat{p}_2 + \sigma_1\left.\frac{\partial\mathscr{N}}{\partial\sigma}\right|_0\hat{p}_1 + \eta_1\left.\frac{\partial\mathscr{N}}{\partial\eta}\right|_0\hat{p}_1, + \sigma_2\left.\frac{\partial\mathscr{N}}{\partial\sigma}\right|_0\hat{p}_0 + \frac{1}{2}\sigma_1^2\left.\frac{\partial^2\mathscr{N}}{\partial\sigma^2}\right|_0\hat{p}_0 + \sigma_1\eta_1\left.\frac{\partial^2\mathscr{N}}{\partial\sigma\partial\eta}\right|_0\hat{p}_0 + \frac{1}{2}\eta_1^2\left.\frac{\partial^2\mathscr{N}}{\partial\eta^2}\right|_0\hat{p}_0. \quad (27)$$

Upon zeroing the terms belonging to each order ($A=0$, $B=0$ and $C=0$), we multiply $\left(\hat{p}_0^\dagger\right)^H$ on the left of B and C. Because $\left(\hat{p}_0^+\right)^H\mathscr{N}(\sigma_0,\eta_0)=0$ for the reference state '0' and recalling that $\mathscr{N}=\mathscr{L}-I\sigma$, we obtain

$$\left(\hat{p}_0^\dagger\right)^H B = \sigma_1\left(\hat{p}_0^+\right)^H\left.\frac{\partial\mathscr{N}}{\partial\sigma}\right|_0\hat{p}_0 + \eta_1\left(\hat{p}_0^+\right)^H\left.\frac{\partial\mathscr{N}}{\partial\eta}\right|_0\hat{p}_0 = 0, \quad (28)$$

$$\left(\hat{p}_0^\dagger\right)^H C = \sigma_1\left(\hat{p}_0^+\right)^H\left.\frac{\partial\mathscr{N}}{\partial\sigma}\right|_0\hat{p}_1 + \eta_1\left(\hat{p}_0^+\right)^H\left.\frac{\partial\mathscr{N}}{\partial\eta}\right|_0\hat{p}_1 + \sigma_2\left(\hat{p}_0^+\right)^H\left.\frac{\partial\mathscr{N}}{\partial\sigma}\right|_0\hat{p}_0 + \frac{1}{2}\sigma_1^2\left(\hat{p}_0^+\right)^H\left.\frac{\partial^2\mathscr{N}}{\partial\sigma^2}\right|_0\hat{p}_0 + \sigma_1\eta_1\left(\hat{p}_0^+\right)^H\left.\frac{\partial^2\mathscr{N}}{\partial\sigma\partial\eta}\right|_0\hat{p}_0 + \frac{1}{2}\eta_1^2\left(\hat{p}_0^+\right)^H\left.\frac{\partial^2\mathscr{N}}{\partial\eta^2}\right|_0\hat{p}_0 = 0. \quad (29)$$

Rearranging Eqns. (28) and (29), yields [8, 10]

$$\sigma_1 = \underbrace{-\frac{\eta_1\left(\hat{p}_0^\dagger\right)^H\left.\frac{\partial\mathscr{N}}{\partial\eta}\right|_0\hat{p}_0}{\left(\hat{p}_0^\dagger\right)^H\left.\frac{\partial\mathscr{N}}{\partial\sigma}\right|_0\hat{p}_0}}_{T1\text{ord}}, \quad (30)$$

$$\sigma_2 = \underbrace{-\frac{\sigma_1\left(\hat{p}_0^+\right)^H\left.\frac{\partial\mathscr{N}}{\partial\sigma}\right|_0\hat{p}_1}{\left(\hat{p}_0^+\right)^H\left.\frac{\partial\mathscr{N}}{\partial\sigma}\right|_0\hat{p}_0}}_{T2\text{ord}(1)} \underbrace{-\frac{\eta_1\left(\hat{p}_0^+\right)^H\left.\frac{\partial\mathscr{N}}{\partial\eta}\right|_0\hat{p}_1}{\left(\hat{p}_0^+\right)^H\left.\frac{\partial\mathscr{N}}{\partial\sigma}\right|_0\hat{p}_0}}_{T2\text{ord}(2)} \underbrace{-\frac{1}{2}\frac{\sigma_1^2\left(\hat{p}_0^+\right)^H\left.\frac{\partial^2\mathscr{N}}{\partial\sigma^2}\right|_0\hat{p}_0}{\left(\hat{p}_0^+\right)^H\left.\frac{\partial\mathscr{N}}{\partial\sigma}\right|_0\hat{p}_0}}_{T2\text{ord}(3)} \underbrace{-\frac{\sigma_1\eta_1\left(\hat{p}_0^+\right)^H\left.\frac{\partial^2\mathscr{N}}{\partial\sigma\partial\eta}\right|_0\hat{p}_0}{\left(\hat{p}_0^+\right)^H\left.\frac{\partial\mathscr{N}}{\partial\sigma}\right|_0\hat{p}_0}}_{T2\text{ord}(4)} \underbrace{-\frac{1}{2}\frac{\eta_1^2\left(\hat{p}_0^+\right)^H\left.\frac{\partial^2\mathscr{N}}{\partial\eta^2}\right|_0\hat{p}_0}{\left(\hat{p}_0^+\right)^H\left.\frac{\partial\mathscr{N}}{\partial\sigma}\right|_0\hat{p}_0}}_{T2\text{ord}(5)}, \quad (31)$$

where $\hat{p}_1$, i.e., the drift of the eigenvector, can be found by solving the singular linear system that results after equating Eqn. (26) to zero

$$\mathscr{N}(\sigma_0,\eta_0)\,\hat{p}_1 = -\sigma_1\left.\frac{\partial\mathscr{N}}{\partial\sigma}\right|_0\hat{p}_0 - \eta_1\left.\frac{\partial\mathscr{N}}{\partial\eta}\right|_0\hat{p}_0. \quad (32)$$

Appendix C: The adjoint thermoacoustic mode

The eigenvalue problem under study $\mathscr{L}\hat{p}=\sigma\hat{p}$ (Eqn. (5)) is related to an adjoint eigenvalue problem that reads

$$\left(\hat{p}^\dagger\right)^H\mathscr{L} = \sigma\left(\hat{p}^\dagger\right)^H, \quad (33)$$

where $\hat{p}^\dagger$ represents the adjoint eigenvector of the thermoacoustic system and H denotes the conjugate transpose. Applying the conjugate transpose to both sides of Eqn. (33), yields

$$\mathscr{L}^H\hat{p}_0^\dagger = \sigma^*\hat{p}_0^\dagger, \quad (34)$$

where * denotes the complex conjugate. The adjoint eigenvector $\hat{p}^\dagger$ can be obtained by solving the eigenvalue problem given by Eqn. (34).

Appendix D: Validation of the in-House Helmholtz solver

The in-house Helmholtz solver was validated against analytical results for simple configurations [24]. For more complex systems, as the one investigated in this work, predictions of eigenfrequencies and eigenmode structures were validated against results provided by AVSP, which is a recognized Helmholtz solver [3]. Figure 10 shows an adaptation of Fig. 8b of Silva et al [4]. These results are obtained when combining a Helmholtz solver with the Flame Describing Function (FDF) of the combustor at operating condition 'B'. This figure represents the growth rate of the first thermoacoustic mode corresponding to the unstable configurations (C03, C04, C08 and C12) for different amplitudes of upstream velocity perturbations. The small mismatch between the in-house Helmholtz solver and AVSP is related to the spatial distribution of the flame within the combustion chamber. Whereas in AVSP a 'V' shape is taken into account, in this work a simpler 'disc-plane' flame is considered. The influence of the flame distribution on results is discussed in section 6.5 of Silva et al. [4]. Table 4 shows the predicted limit cycle amplitude and resonance frequencies obtained by both AVSP and the in-house Helmholtz solver. Experimental results are also shown.

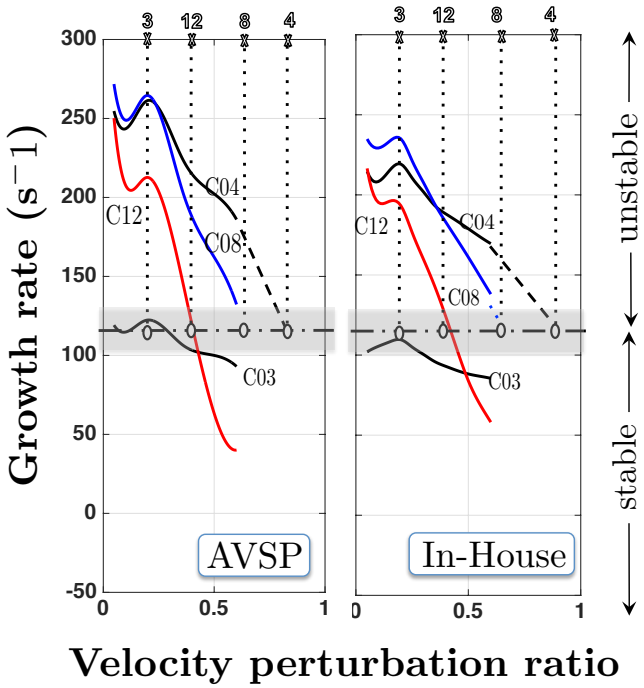

FIGURE 10. Growth rate trajectories as a function of velocity perturbation ratio $|\hat{u}|/\bar{u}_b$ at the flame base (flame B of Palies et al. [19]). The dashed-dotted lines surrounded by the gray band indicate the region where the growth rate is balanced by damping. Crosses indicate the amplitude at which limit cycles are expected. AVSP data taken from Silva et al. [4]

TABLE 4. Resonance frequencies, f, and Limit cycle amplitudes (or velocity perturbation ratios). Results obtained with the in-house Helmholtz solver do not have a subscript. Experimental data ('Exp') and AVSP results taken from Silva et al. [4]

Case	f_{Exp}	f_{AVSP}	f	$\left(\frac{\lvert\hat{u}\rvert}{\bar{u}_b}\right)_{\text{Exp}}$	$\left(\frac{\lvert\hat{u}\rvert}{\bar{u}_b}\right)_{\text{AVSP}}$	$\left(\frac{\lvert\hat{u}\rvert}{\bar{u}_b}\right)$
C03	143	150	159	0.3	0.2	0.2
C04	140	147	152	0.9	0.8	0.9
C08	126	136	139	0.7	0.6	0.65
C12	128	129	132	0.5	0.4	0.4